Band Offset Models of Semiconductors and Insulators

Y Guo, H Li, S J Clark, J Robertson,

School of Engineering, Swansea University, Swansea, UK
Engineering Dept, Cambridge University, Cambridge CB3 0FA, UK
Physics Dept, Durham University, Durham, UK

Abstract The band offsets at a heterojunction lies between two limits, those given by the electron affinity rule and the matching of the charge neutrality levels (CNLs) or branch point energies. It is shown that it has been difficult to compare these cases because most experimental and theoretical tests require a lattice-matching across the heterojunction, and most semiconductors with the same lattice constant have similar average band energies referenced to the vacuum level. A second point is that the CNL when referenced to the vacuum level varies surprisingly weakly with the midgap energy referenced to the vacuum level. A calculation of band offsets for larger lattice mismatch heterojunctions provides a strong test, whose result is found to favour the CNL matching model. This result is important for the majority of practical device heterojunctions, where there is no match due to poly-crystallinity or other effects. For other cases whether the device consists of molecules, the electron affinity rule holds.

Introduction

Most semiconductor devices require a knowledge of the band alignment at the heterojunctions within them, whether these are between two semiconductors, between a semiconductor and an insulator, or the Schottky barrier interface between a metal electrode and a semiconductor. The band offsets can be derived by using density functional calculations on representative atomic models of the heterojunction [1-10]. However, in general this can be difficult unless the two components are well lattice-matched, otherwise this can require large supercell periodicities along the interface to ensure commensurate lattices, which may involve many atoms in the overall supercell or an interface with mismatch defects like dangling bonds. This particularly applies to systems like solar cells, light emitting materials, quantum dots, or thin film transistors, where the materials involved can be poly-crystalline or even amorphous. Thus, there is also a desire for a simplifying principle or model that predicts band offsets under more general conditions of poor lattice-matching.

In broad terms, there are two limiting models for the band offset [1-11]. The first 'natural' band offset is if there is no charge transfer across an interface and so the conduction band offset is simply the difference between two energies of the two semiconductors such as electron affinities, as in the electron affinity model [1-3]. This model holds for molecular semiconductors where the inter-molecular bonding is van der Waals, which allows only minimal charge transfer [12]. The second limit, as in inorganic macromolecule semiconductors, is that the offset depends strongly on the charge transfer across the interface, so that the 'bare' band offset is screened by the charge transfer across the interface [4-7]. These limits are related respectively to the unpinned (Schottky) and pinned (Bardeen) limits of Schottky barriers [5,11,13,14]. While the behaviour of Schottky barriers is reasonably well understood, this is less so for semiconductor heterojunctions [8,9], even allowing for the effects of shallow cation d levels [15]. Although studied for over 40 years, the validity of these limits applied to such heterojunctions is less

settled. Here, we show why testing these limits has been less decisive. To do this, we investigate some specific semiconductor pairs with larger lattice mismatches. The results of this favor the charge neutrality level (CNL) model. We cover four broad classes of materials, the 3-dimensionally bonded semiconductors like Si and GaAs, the insulators like HfO_2, the transparent conductors like SnO_2 and the 2D semiconductors like MoS_2.

As a preliminary, we note that in order to test band offsets, we must have accurate values for the band gaps themselves [16-18]. We use hybrid functionals to correct the band gap error of the standard semi-local forms of density functional theory (DFT). It is conventional to judge the quality of a particular hybrid functional method in terms of how accurately they predict the band gap. Here we note that in discussing band offsets, the quality of prediction of both band gaps and electron affinities should be judged on an equal weight.

Methods

The band gap, electron affinity (EA), and ionization potential (IP) of each semiconductor system are calculated here using a supercell model containing a slab of 8 layers of semiconductor and a 20Å of vacuum layer. In each case the semiconductor slab is terminated by a non-polar surface. The electrostatic potential in the vacuum region is used to define the vacuum level energy. For the direct calculations of band offsets, we use supercells containing 6 layers of each semiconductor joined by their non-polar surfaces, both with and without a vacuum layer.

The calculations are carried out using the plane wave pseudopotential code CASTEP [19]. The atomic geometries are relaxed within the PBE version of GGA. In this case, ultrasoft pseudopotentials are used with a plane wave cutoff of 400 eV, which converges the total energy to within 0.01 eV per atom. A 5x5x1 MP k-point mesh is used for geometry optimization. The residual force is less than 0.02eV/Å. A 11x11x1 k-point mesh is used to calculate the density of states. For layered compounds, the Grimme [20] dispersion correction is used to correct the DFT error for the van der Waals interaction and the associated bond lengths. Spin-orbit coupling is not included.

For both 3D and layered compounds, the band gap error of the generalised gradient approximation (GGA) of DFT is corrected by using hybrid functionals, such as the Heyd-Scuseria-Ernzerhof (HSE)[21] functional or screened exchange (sX) hybrid functional [22]. In this case, norm-conserving pseudopotentials were used with an energy cutoff of 750 eV.

Results

A Band Gaps and Electron Affinities

The GGA band gap error can be corrected using hybrid density functionals. Two well known methods are the Heyd-Scuseria-Ernzerhof (HSE) functional [21], and the screened exchange (SX) functional [22]. These functionals mix a certain fraction of screened Hartree-Fock exchange into the DFT exchange-correlation density functional. The hybrid functionals are not a parameter-free means of correcting the DFT band gap error as, amongst other possibilities, the fraction of screened exchange can be fitted. The calculated band gap for various compounds is given for HSE by Hinuma et al [8] and Chen et al [17,18] and for SX by Clark and Robertson [22]. These show that the SX band gaps match the experimental gaps over the full range of band gaps. On the other hand, the HSE band gaps match well for a smaller range of gaps but then they decline for very large gaps. This aspect can be adjusted by varying the fraction of exact exchange

mixed into the exchange-correlation functional. One way would be to ensure the linearity of the total energy with fractional occupation across the band gap [23]. Another way is vary the fraction of exchange included in proportion to the inverse optical dielectric constant [24,25], as was done by Marques et al [25] and then by Chen [18]. It is pointed out here that, in terms of band offsets, the electron affinity as well as the band gap should be used to judge the fraction of exchange to be included.

Chen [17] and others have checked the alignment of hybrid functional band energies with those of GGA and with each other using the calculated electrostatic potential of the bulk semiconductors. In the case of SX, this is equivalent to the calculated ionisation potential, where the vacuum potential is used as the reference level.

Fig. 1 compares the calculated GGA and SX band gaps against the experimental values. Table A1 compares the calculated band gaps and electron affinities of the various tetrahedrally bonded semiconductors calculated with the SX functional. These are compared with their experimental values from the compilation of Brillson [26].

Fig. 2 shows the variation of the GGA and SX values of electron affinity and ionisation potentials for the various semiconductors. We see that the SX values are wider than the GGA values for both valence and conduction bands.

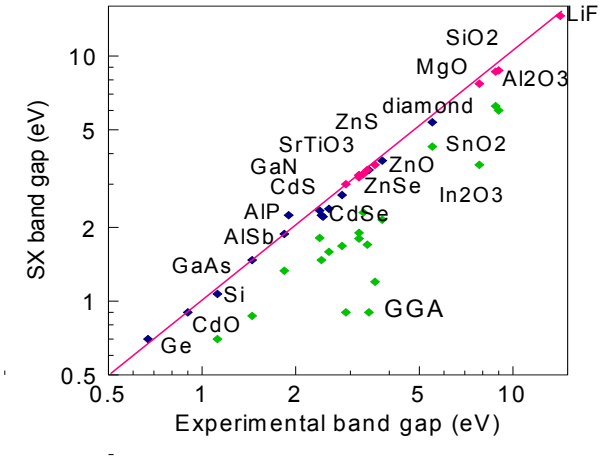

Fig. 1. Variation of calculated band gap with experimental gap, showing calculated GGA and SX gaps [22].

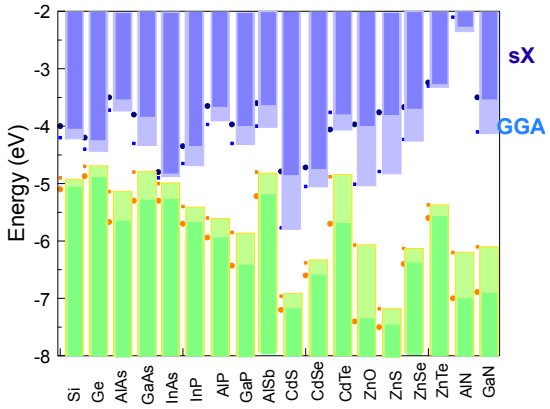

Fig. 2. The calculated electron affinity and ionisation potentials for tetrahedral semiconductors, in the GGA and SX functionals.

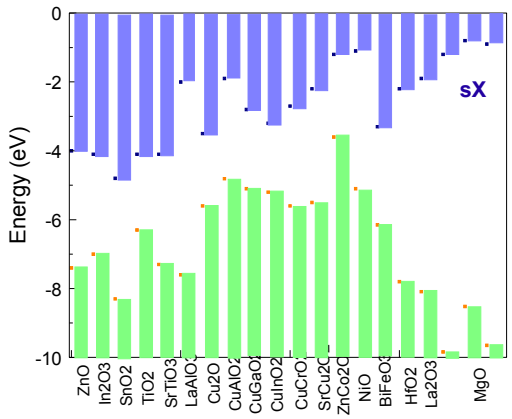

Fig. 3. Calculated electron affinities and ionisation potentials for various oxides, using the SX functional.

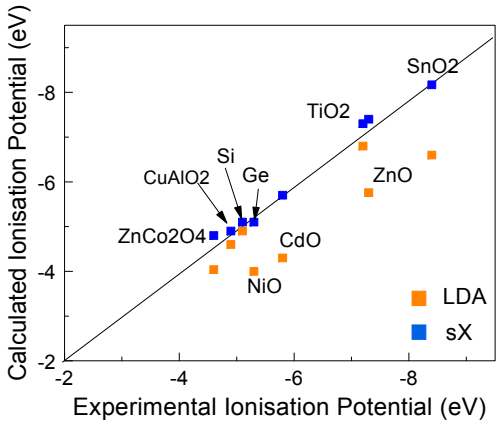

Fig. 4. Calculated GGA and SX values of ionisation potential vs. their experimental values for some oxides.

We now consider various functional oxides such as the transparent conducting oxides (TCOs) used in displays and solar cells, and the high K oxides used as gate dielectrics in CMOS. Table 2 gives the calculated band gaps, electron affinities and ionisation potentials of such oxides compared to their experimental values from compilations of Hosono [27], Klein [28], Hattori [29], Greiner [30] and Robertson [31].

Table A2 gives the calculated SX electron affinities, ionization potentials and band gaps, and compares them to the experimental values. Fig 3 shows the calculated SX electron affinities and ionisation potentials for various oxides, both conducting and non-conducting. Fig. 4 compares the calculated ionisation potentials of some oxides with their experimental values. Whereas the GGA band gap is typically a 30% under-estimate for semiconductors, there can be a much larger error of up to 75% for the TCOs.

For many technologically important systems like the TCOs, the band gap error can be particularly large and it arises from two separate effects. The first is the direct semi-local DFT under-estimation of the VB-CB gap, while the second is the effect of semi-core levels of the cations. This occurs for post-transition metal cations such as Zn, Cd and In. Here the upper valence states consist of anion p states and these are repelled upwards by the cation semi-core

states [15,32]. Self-interaction causes the semi-core states to be too high in GGA, and they have repelled the VBM which lies too high. The hybrid functionals will move the core states down in energy and so lessen their repulsion of the VBM state. This effect occurs in the n-type TCO compounds like ZnO and In_2O_3, in the solar cell compounds like $CuInSe_2$ [32-35].

As an example, Fig. 5 shows the development of the band edge energies of ZnO from GGA to HSE to SX and compared to experiment. It is seen that HSE for the standard mixing fraction of $\alpha = 0.25$ has a gap of only 2.3 eV and it opens considerably more on the CBM side by moving to SX. SX has improved the VB energy because it has moved the Zn 3d states down more [35].

Fig. 5(b) shows this in a different way. The band gap of ZnO opens up as the TF screening parameter reduces, with the VBM and CBM moving away symmetrically from the gap center. On the other hand the Zn 3d level moves downwards, but it keeps a relatively constant energy below the VBM. Thus, if a parameter tuning scheme is desired for hybrid functionals, varying the value of alpha will widen the band gap, but the Zn 3d depth below the VBM is relatively unchanged [31]. Thus, in this scheme there is nothing to vary the Zn 3d depth independently.

We see that our band energies are similar to those of Stephanovic [33]. On the other hand, there are differences to the well known compilation of van der Walle and Neugebauer [36] (eg ZnO vs ZnS). This is mainly because the latter authors used the GGA+U method as a solution for band energies.

Many p-type TCOs are Cu oxide compounds [37,38]. The Cu 3d states lie at similar energies to the O 2p states, and their interaction lowers the effective mass of the O 2p states when they form the upper valence band. A number of p-type TCOs are from the defossalite family of hexagonal layer compounds [39-41]. Here we choose the (1101) faces as the nonpolar faces. The defossalites are notable for having a main optical absorption edge which is significantly above the minimum gap due to low optical matrix elements.

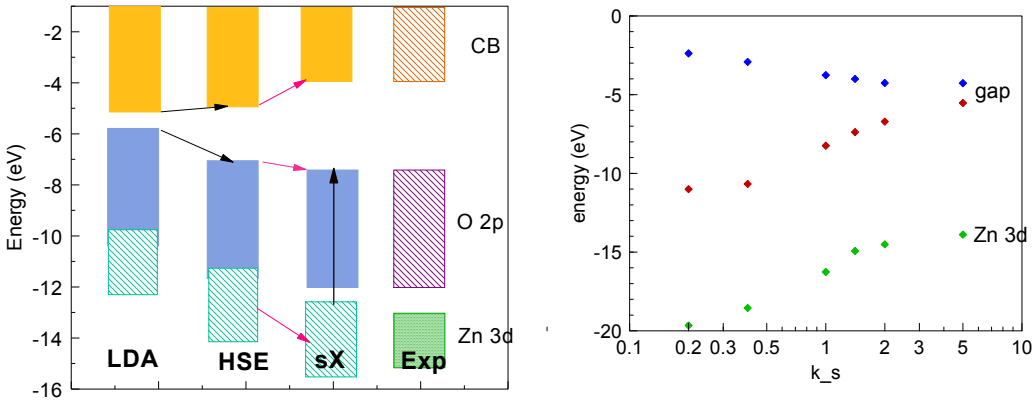

Fig. 5. Development of the valence band maximum, conduction band minimum and Zn 3d core levels, from LDA to HSE to SX, compared to experiment. (b) Variation of valence band maximum, conduction band minimum and Zn 3d core level of ZnO with SX screening constant. k_s is typically 1 $Å^{-1}$.

The high K oxides used as gate dielectrics are all closed shell wide band gap systems. The metals are very electropositive so the oxides have a high heat of formation, so that the oxides cannot be reduced by reaction with Si. They include the oxides of Hf, Zr, La, Y, Sc, Lu, Sr, and

Ba [11,31,42]. The rare-earth oxides such as Gd_2O_3 are also possible high K oxides [43], if their 4f states are out of the gap. On the other hand, TiO_2, $SrTiO_3$ and Ta_2O_5 do not have a sufficiently high heat of formation and can react with Si [11]. All these oxides have a roughly 30% band gap error.

$BiFeO_3$ is an interesting multiferroic oxide [44], where Fe is the magnetic ion, and Bi is the ferroelectric ion, where the distortion polarises its 6s lone pair state. $BiFeO_3$ has the R_{3c} crystal structure, and its antiferromagnetism is aligned along its z-axis.

NiO is representative of another family of p-type oxides [45]. It is an open shell oxide with a wide Ni 3d –like upper valence band. It has the rocksalt structure, with its antiferromagnetic along the z-axis as in $BiFeO_3$.

Charge Neutrality Level

The vacuum level acts as a reference level in the electron affinity rule. In the charge transfer model, the reference level which controls the charge transfer across an interface is the charge neutrality level (CNL) of the semiconductor. The charge transfer across a semiconductor heterojunction in Tersoff's model depends on the evanescent states of the narrower gap side decaying into the gap on the larger gap side [4]. These evanescent states are the analogues of the metal induced gap states (MIGS) at the metal-semiconductor interface (Schottky barrier). The MIGS are intrinsic to the semiconductor side and represent a smearing of the surface states on a free semiconductor surface. The CNL is the energy at which the MIGS are filled up to for a neutral surface. They are also the branch point of the complex band structure in the gap.

The CNL can be calculated from the bulk band structure from the zero of its Greens function [4,46-50,11],

$$G(E) = \int_{-\infty}^{\infty} \frac{N(E').dE'}{E - E'} = 0 \qquad (1)$$

The integral is taken over the Brillouin zone and the sum is over all bands.

A key question is how many valence or conduction bands should be included in the integral. In the original expression, the limits on the number of bands were infinite. The integral becomes convergent by including the wavefunctions in the integral, as was done in the original Tersoff formulation [4]. Initially, we used an atomic orbital basis set for the calculation of CNLs [11]. When using a plane wave basis set, we included only the same bands as in a tight-binding description [31,48], that is four valence bands and four conduction bands for a zincblende semiconductor, and the equivalent for other lattices or d-band compounds [48]. A similar counting was used by others [46]. In practice the resulting CNL values for wide gap oxides were relatively insensitive to the choice.

However, this choice was less appropriate for semiconductors with wider bands where the convergence was poor. Schliefe et al [49,50] used fewer bands when calculating the CNLs of tetrahedral semiconductors, and this gave values slightly closer to those of other formulations such as the Cardona method [51]. The latter choice is supported if one inspects the imaginary band structure of various systems [52,53], where the branch point is taken from the bands closest to k=0. For HfO_2, four bands is a good choice [54], but for semiconductors, one band is clearly

much closer to k=0 than others [52,53]. Hence, here we now include fewer bands than previously for the CNL calculation.

Band Offsets

The heterojunctions of two semiconductors are constructed by joining them by a non-polar surface, such as (110) for zincblende structures. The band offsets are then given by the linear model as [11],

$$\phi_n = (\chi_a - \Phi_{CNL,a}) - (\chi_b - \Phi_{CNL,b}) + S(\Phi_{CNL,a} - \Phi_{CNL,b}) \quad (2)$$

Here ϕ_n is the conduction band offset, χ_a is the electron affinity of *a*, $\Phi_{CNL,a}$ is the CNL of *a*, and S is the pinning factor. This is an extension of the Cowley-Sze model [55] of Schottky barriers to heterojunctions.

The two limits of the electron affinity rule and the CNL matching rule can be regarded as using an external reference energy (the vacuum level) or an internal reference level of the semiconductor (the CNL/branch point of its bulk band structure). These points were realised in 1986 when Harrison [3] proposed that band offsets should be referenced to the vacuum level in his tight-binding analysis, and then Harrison and Tersoff [6] over-ruled this model when realising that screened band offsets should be used. At the time, the numerical inaccuracies of the tight-binding analysis distracted from the validity of this argument.

Experimental [56,57] and theoretical supercell tests [8,9,10,58] of these two limits require lattice-matching of the two sides. To an extent, strain can be used to match the two components, and then the effect of the strain adjusted for in the energies with respect to the vacuum level. On the other hand, a more direct, significant test would involve two components whose band energies are likely to lead to significant charge transfer.

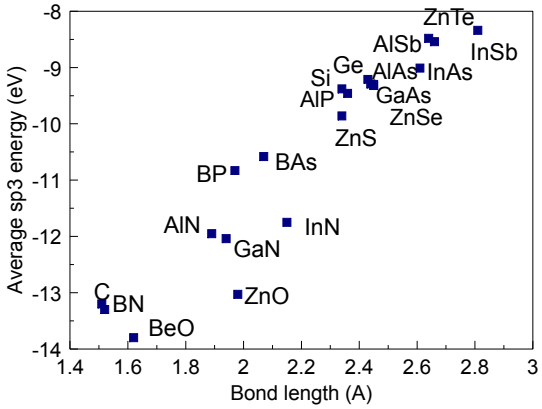

Fig. 6. The strong correlation between the sp^3 hybrid energy in tight-binding and bond length of the various tetrahedrally-bonded semiconductors

Fig. 6 shows the variation of the average sp^3 orbital energy (from the atomic orbital energies) vs. the bond lengths for the tetrahedrally bonded binary semiconductors. These show a close correlation between the average sp^3 energy and the bond length. Thus by requiring lattice matching, one chooses pairs of semiconductors of similar average sp^3 energy, and so are unlikely to have a large charge transfer across the interfacial bonds, as Harrison and Tersoff [6] noted.

A second point concerns the CNL values that enter into CNL matching limit. Fig. 7 shows the variation of CNL energies referred to the vacuum level versus the average of the electron affinity and ionisation potentials (the midgap energy). The data are fitted by a line of slope S=0.34. This means that the CNL does not lie at a constant fraction of the band gap, but has a trend that if the average band gap energy moves down, away from the vacuum level, the CNL energy upwards in the gap, to give much less overall shift than might be expected. A similar effect occurs in oxides in Fig. 8 [37], where the data is more scattered but has a similar trend.

Thus, a comparison of heterojunctions for the two limits using lattice-matched pairs [8,9,56] will not give as great a difference of band offsets as might be expected.

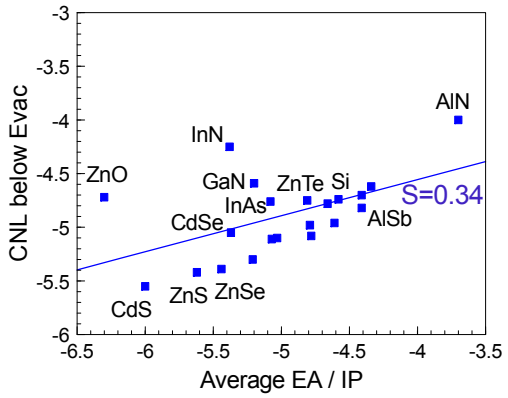

Fig. 7. The weak variation of the CNL energy (wrt. vacuum level) vs. the average of electron affinity and ionisation potential for the tetrahedral semiconductors. Slope = 0.34

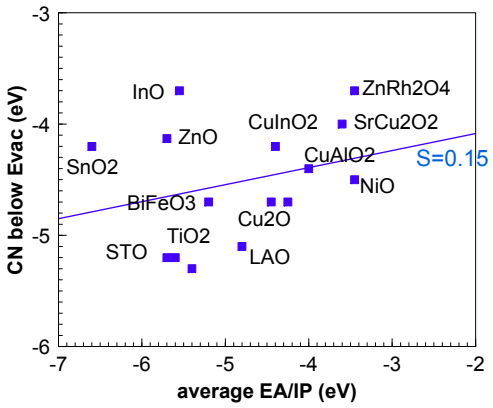

Fig. 8. Variation of the CNL energy wrt. vacuum level vs. the average of electron affinity and ionisation potential for various oxides. The slope of the line is 0.15.

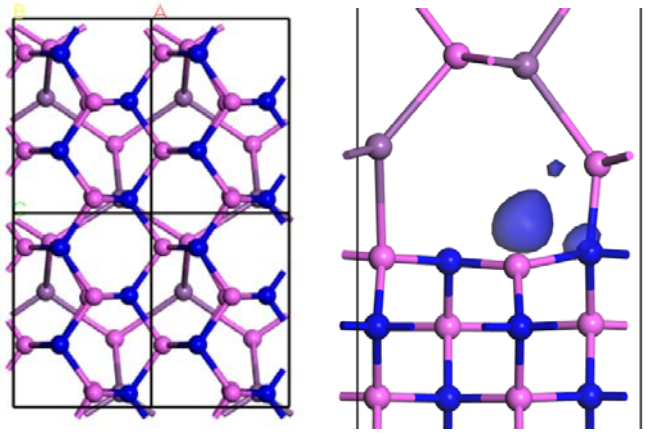

Fig. 9. Top and side view of the model zincblende (110)AlN:AlSb heterojunction with a √2:1 lattice-matching. N= blue, Al= pink, Sb=brown.

In order to test the two limits with a stronger choice, we do not consider band offsets of lattice-matched pairs, but between pairs with a large mismatch of √2. The surface unit cell of (110) is √2 x 1, so that it is a possible to match lattices of ratio √2 if the second lattice is rotated by 90^0, as shown in Fig 9. Fig 9(b) illustrates a side-view of bonding at such an interface. We consider a supercell consisting of 6 layers of each semiconductor. The chosen pairs are AlSb or ZnTe for the larger lattice, and AlN, GaN and ZnO for the smaller lattice. The side-view shows that not all of the bonds continue across the interface, there are some dangling bonds left on the short lattice side. However, these are pairs of cation and anion DBs which relax and have charge transfer between them, so that they do not form gap states (Figs. 9b,10).

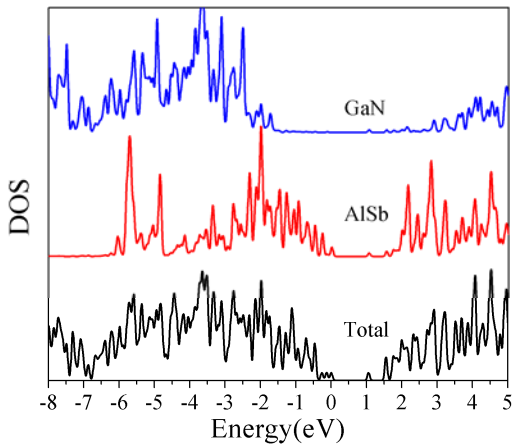

Fig. 10. Partial density of states in SX for GaN and AlSb layers at the (110)GaN:AlSb heterojunction. Note the absence of gap states.

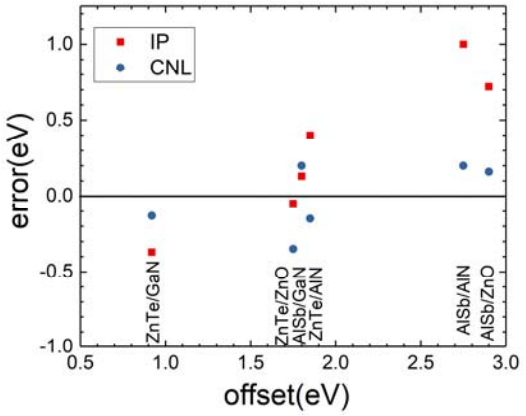

Fig. 11. Error between the calculated VB offsets at heterojunctions and estimated VBO values using the EA/IP rule (red) and the CNL matching rule (blue).

AlSb and AlN are seen to have different CNL energies from Fig. 7. Fig. 10 shows the calculated local density of states for atomic layer away from the interface in the SX hybrid functional. The valence band offsets VBO can be read off from Fig. 10 as the difference of the intercept of the PDOS with the energy axis. The VBO values for the six interfaces ZnTe:GaN, ZnTe:AlN, ZnTe:ZnO, AlSb:GaN, AlSb:AlN and AlSb:ZnO are listed in Table 1. The difference of this VBO value from the CNL difference (blue) or the IP difference (red), or 'error', is plotted against the calculated supercell VBO on the horizontal axis in Fig 11. The VBO difference for the case of the CNL rule can be derived from eqn (2) using S=0, because the dielectric constants of ZnTe and AlSb as large, so that S is very small. We note that the blue points cluster closer to the horizontal axis than the red points. This shows that the data is more consistent with the CNL matching limit overall although there is some error in the CNL points. The error could result from two factors, first that the test systems ZnO and ZeTe had shallow cation cores, and second, the effect of the dangling bonds at the interface as in Fig 9.

	Supercell calculation (eV)	IP difference (eV)	IP error (eV)	CNL difference (eV)	CNL error (eV)
AlSb/GaN	1.8	1.7	-0.28	1.6	-0.11
AlSb/AlN	2.75	1.8	-0.42	2.6	-0.05
AlSb/ZnO	2.9	2.2	-0.17	2.8	-0.03
ZnTe/GaN	0.92	1.3	0.41	1.0	0.09
ZnTe/AlN	1.85	1.4	-0.24	2.0	0.08
ZnTe/Zno	1.75	1.8	0.03	2.2	0.26

Table 1. Comparison of the valence band offsets calculated from the supercell model, and from the electron affinity (IP) rule, and from the CNL matching rule, and the errors from the supercell calculation in each model. IP values are those calculated by SX.

2D materials

Heterojunctions of the transition metal dichalcogenides (TMDs) and similar semiconductors have been studied for many applications, including the tunnel field effect transistor (TFET). The TFET is a transistor design with a particularly sharp turn-on characteristic or 'steep slope' needed for low power computation [59]. TFETs will use the heterojunction between vertically stacked layers of different TMDs with a type II / III band alignment. The advantage here is that the van der Waals bonding between the layers does not require the layers to be lattice matched, so that in principle a heterojunction without defects is possible. This differs from a typical heterojunction between III-V semiconductors which often have mismatch defects which degrade the turn-on characteristic.

It is also possible to make the lateral heterojunction where the layers of the two compounds are directly bonded to each other. Interestingly, reasonably abrupt HJs have been achieved between TMDs for this case, even when not fully lattice matched.

The band energies of these semiconductors with respect to the vacuum level have been calculated by various workers [59-61]. The electron affinities, ionisation potentials, and charge neutrality levels have been calculated for both bulk and monolayer versions in the SX functional [61]. The values for the monolayers is shown in Fig. 12. It is notable in Fig. 12 that the CNL energy referred to the vacuum level *does* vary between these compounds, and thus does not follow the behaviour of the 3D semiconductors seen in Fig. 7. This is very interesting. It shows that the 'balancing' process as occurs in 3D semiconductors is not seen in TMD semiconductors. The band offsets for stacked heterojunctions are assumed to obey the electron affinity rule, and tests indicate that this is broadly true.

On the other hand, lateral heterojunctions, being fully bonded, are essentially the same as heterojunctions of 3D semiconductors. It has been tested whether they follow the CNL matching rule or the electron affinity rule by calculating the band offsets using supercell calculations. Generally, it is found that they do obey the CNL matching rule [61,62], as summarised in Fig. 13. It is not yet clear if there has been a good experimental test of this behaviour. Nevertheless, Fig. 13 indicates that 2D semiconductors present a good test of both the no charge transfer and screened limits for band offsets at heterojunctions.

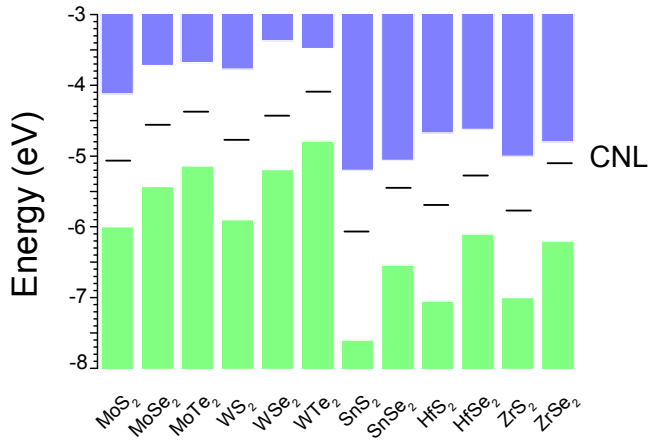

Fig. 12. Electron affinities, ionisation potentials and CNLs of various metal dichalcogenides calculated by the SX functional.

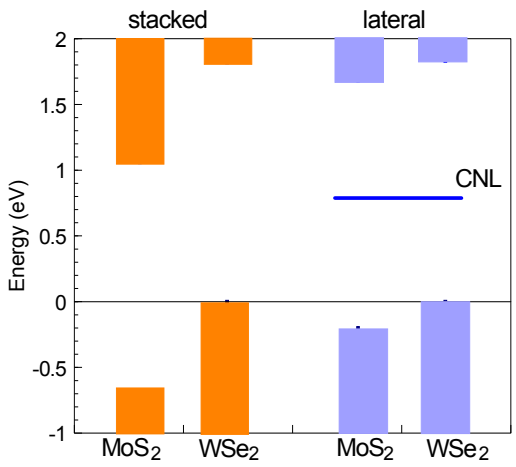

Fig. 13. Comparison of the band alignments for stacked and lateral junctions, calculated for supercells.

Discussion

The weak dependence of the CNL energy on the average of the electron affinity and ionisation potentials from Fig. 7 helps to explain a number of other diverse effects.

The first effect is the behaviour of interstitial hydrogen in semiconductors. Hydrogen can have two basic behaviours [36,63,64], (a) as a shallow donor, with its +1/0 and 0/ -1 levels lying at the CBM, (b) as a deep amphoteric defect with its +1/0 and 0/-1 levels deep in the gap, and usually showing a 'negative-U' property. In the tetrahedral semiconductors, van der Walle and Neugebauer [36] showed the remarkable property that interstitial hydrogen's +1/-1 level lay at an almost constant energy below the vacuum level for all these semiconductors, and including SiO_2 and water. This result implies that there is a constant reference energy for H, the vacuum level. A similar result but with more scatter is found to occur for interstitial hydrogen in oxides [63].

Van de Walle and Neugebauer [36] explained this behavior of hydrogen as a breaking of a C-A bond (c=cation, a=anion), with H bonding to the C in the +1 state and H bonding to the A in the -1 state. The sites with a bonded hydrogen would have four bonds and so be passivated, leaving a cation dangling bond for the +1 state and an anion dangling bond for the -1 state. The overall result would be that the +1/-1 transition level would lie the average energy of the cation and anion DBs, which is similar to the CNL energy. Thus, this mechanism would argue for the +1/-1 state would be roughly the CNL energy, and not particularly related to the vacuum level. Only in the case of water should there be a relationship to the vacuum level via the electrochemical series. However, if, for a narrow set of semiconductors, the CNL energy actually varies little, as occurs in Fig 7, then the vacuum level could act as a reasonable reference energy.

The second effect is doping limits. It was found empirically that the maximum dopant concentration in a semiconductor corresponded to it being able to move its Fermi energy only within certain energy limits, on either the n- or p-type side [65]. Beyond that, the dopant makes compensated defect complexes which stop further movement of E_F. If these energies are within the band gap rather than in the bands, then that semiconductor cannot be doped for that polarity. An energetic analysis of this behaviour showed that the dopant becomes compensated by an intrinsic defect of the opposite sign, and the doping limit then corresponds to an E_F where the

compensating defect will form spontaneously. The defect have a zero formation energy at this E_f value [66]. Should these doping limit energies be constant with respect to a particular semiconductor's reference energy, such as its CNL, or should they be relatively independent of material and referred to the vacuum level? It turns out that it is difficult to differentiate between these two cases using the available data [37]. Fig. 7 provides some resolution to this question, because the CNL energy does not vary so much with the average of EA and IP, so both cases can hold at the same time. It will need better data, calculations, or a special materials system to differentiate between these two cases.

Conclusions

DFT supercell calculations are used to calculate the band offsets at semiconductor heterojunctions and if these follow two extreme limits, the electron affinity rule (no chrge transfer) and the CNL matching rule (finite charge transfer). It is shown that traditional tests of these limits are not very strong because average band energies have a strong correlation with average bond lengths, so tests between lattice-matched heterojunctions are not a strong test. By using the case of a 1.41 lattice-mismatch, this provides a stronger test, which is found to support the CNL matching case.

The fact that in most macromolecular semiconductors that the CNL lies at a relatively constant energy below the vacuum level explains two other observations, that the +1/-1 energy level of the interstitial hydrogen should lie at a relatively constant energy, also that the doping limits lie at relatively constant energies below the vacuum level.

Appendix

Table A1. Calculated SX values of band gap, electron affinity, ionization potential, charge neutrality level, and their experimental values, for 8-electron semiconductors.

eV	Gap, SX	EA, SX	CNL, SX	CNL	Gap, exp	EA, exp
Si	1.10	-4.00	-5.10	0.20	1.11	-4.05
Ge	0.67	-4.20	-4.87	0.10	0.67	-4.00
AlAs	2.17	-3.50	-5.67	0.85	2.16	-3.50
GaAs	1.50	-3.80	-5.30	0.50	1.43	-4.07
InAs	0.50	-4.80	-5.30	0.45	0.36	-4.90
InP	1.35	-4.35	-5.70	0.93	1.35	-4.35
GaP	2.29	-3.65	-5.94	0.83	2.26	-3.65
AlP	2.46	-3.97	-6.43	1.30	2.45	-3.98
AlSb	1.62	-3.60	-5.22	0.53	1.60	-3.60
CdS	2.41	-4.79	-7.20	1.90	2.42	-4.79
CdSe	1.88	-4.72	-6.60	1.50	1.73	-4.50
CdTe	1.64	-4.06	-5.70	1.12	1.58	-4.28
ZnO	3.43	-3.97	-7.40	3.27	3.39	-4.20
ZnS	3.74	-3.76	-7.50	1.75	3.60	-3.82
ZnSe	2.73	-3.67	-6.40	1.60	2.70	-4.09
ZnTe	2.36	-3.24	-5.60	1.09	2.25	-3.53
AlN	6.20	-0.80	-7.00	3.08	6.20	-0.60
GaN	3.39	-3.50	-6.89	2.14	3.20	-3.30

Table A2. Calculated SX values of band gap, electron affinity, and ionization potential for various oxides, and their experimental values.

eV	Gap, SX	EA, SX	IP, SX	CNL	Gap, exp	EA, exp
ZnO	3.40	-4.00	-7.40	3.27	3.40	-4.1
In_2O_3	2.70	-4.10	-7.00	3.30	2.60	-4.1
SnO_2	3.60	-4.80	-8.30	4.10	3.60	-4.8
TiO_2	3.20	-4.10	-6.30	2.20	3.20	-4.1
STO	3.20	-4.10	-7.30	2.60	3.20	-4.1
LAO	5.60	-2.00	-7.60	3.80	5.60	-2
Cu_2O	2.10	-3.50	-5.60	0.80	2.10	-3.5
$CuAlO_2$	2.80	-1.90	-4.81	0.90	3.00	-1.9
$CuGaO_2$	2.30	-2.80	-5.10	0.80	2.40	-2.8
$CuInO_2$	2.00	-3.20	-5.20	0.80	2.00	-3.2
$CuCrO_2$	2.90	-2.70	-5.60	1.10	3.00	-2.7
$SrCu_2O_2$	3.30	-2.20	-5.50	2.00	3.00	-2.2
$ZnCo_2O_4$	2.36	-1.20	-3.60	2.40	2.30	-1.2
NiO	3.50	-1.10	-5.10	1.80	4.10	-1.1
$BiFeO_3$	2.85	-3.30	-6.15	1.90	2.80	-3.3
HfO2	5.60	-2.20	-7.80	3.70	5.80	-2.2
La_2O_3	6.19	-1.90	-8.09	2.40	6.10	-1.9

Al_2O_3	8.64	-1.20	-9.84	5.50	8.80	-1.2
MgO	7.72	-0.80	-8.52	4.00	7.80	-0.8
SiO_2	8.75	-0.90	-9.65	4.50	9.00	-0.9

References

1. C G van de Walle, R M Martin, Phys Rev B 35 8154 (1987)
2. S H Wei, A Zunger, App Phys Lett 72 2011 (1998)
3. W A Harrison, J Vac Sci Technol 14 1016 (1977)
4. J Tersoff, Phys Rev B 30 4874 (1984)
5. J Tersoff, Phys Rev Lett 52 465 (1984); J Vac Sci Technol B 4 1068 (1986)
6. W A Harrison, J Tersoff, J Vac Sci Technol B 4 1068 (1986)
7. A Baldereschi, S Baroni, R Resta, Phys Rev Lett 61 734 (1988)
8. Y Hinuma, A Gruneis, G Kresse, F Oba, Phys Rev B 90 155406 (2014)
9. Y Hinuma, Y Kumagai, I Tanaka, F Oba, Phys Rev B 95 075302 (2017)
10. K Steiner, W Chen, A Pasquarello, Phys Rev B 89 205309 (2014)
11. J Robertson, J Vac Sci Technol B (2000)
12. J Hwang, A Wan, A Kahn, Mater Sci Eng R 64 1 (2009)
13. W Monch, Phys Rev Lett 58 1260 (1987)
14. R T Tung, Phys Rev Lett 84 6078 (2000)
15. S H Wei, A Zunger, Phys Rev Lett 59 144 (1987)
16. F Oba, Y Kumagai, App Phys Express 11 060101 (2018)
17. W Chen, A Pasquarello, Phys Rev B 88 115104 (2013)
18. W Chen, G Miceli, G M Rignanese, A Pasquarello, Phys Rev Mats 2 073803 (2018)
19. S J Clark, et al, Zeitschrift Krystallogr 220 567 (2005)
20. S Grimme, J Comput Chem 27 1787 (2006)
21. J Heyd, G E Scuseria, M Erzerhof, J Chem Phys 124 219906 (2006)
22. S J Clark, J Robertson, Phys Rev B 82 085208 (2010); K Xiong, J Robertson, M C Gibson, S J Clark, App Phys Lett 87 183505 (2005)
23. S Lany, A Zunger, Phys Rev B 80 085202 (2009)
24. H P Komsa, P Broqvist, A Pasquarello, Phys Rev B 81 205118 (2010)
25. M A L Marques, J Vidal, M J T Oliveira, L Reining, S Botti, Phys Rev B 83 035119 (2011) hse gap
26. L Brillson, 'Surfaces and Interfaces of Electronic Materials', (Wiley-VCH, 2010) p549.
27. H Hosono, Jpn J App Phys 52 090001 (2013)
28. A Klein, J Am Ceram Soc 99 369 (2016); S Li, et al, Phys Stat Solidi RRL 8 571 (2014); A Klein, J Phys Cond Mat 27 13201 (2015); A Klein, Thin Solid Films 520 3721 (2012)
29. T Hattori, et al, Microelectronic Engineering, 72 283 (2004); K Kakushima et al, in 'Rare earth oxide thin films', ed M Fanciulli, G Scarel, (Springer 2007) p 345
30. M T Greiner, M G Helander, W M Tang, Z B Wang, J Qiu, Z H Lu, Nature Mats 11 76 (2011)
31. J Robertson, J Vac Sci Technol A 31 050821 (2013) cbo
32. F Oba, A Togo, I Tanaka, J Paier, G Kresse, Phys Rev B 77 245202 (2008)
33. V Stefanovic, S Lany, D S Ginley, W Tumas, A Zunger, Phys Chem Chem Phys 16 3706 (2014)
34. Y H Li, A Walsh, S Y Chen, W J Yin, J H Yang, J B Li, J L F DaSilva, X G Gong, S H Wei, App Phys Lett 94 212109 (2009)
35. Y Guo, J Robertson, S J Clark, J Phys Conden Mat 27 025501 (2015)
36. C G van der Walle, J Neugebauer, Nature 423 626 (2003)
37. J Robertson, S J Clark, Phys Rev B 83 075205 (2011)
38. D O Scanlon, G W Watson, J Phys Chem Lett 1 2582 (2010)

39. R Gillen, J Robertson, Phys Rev B 84 035125 (2011)
40. X Nie, S H Wei, S B Zhang, Phys Rev Lett 88 066405 (2002);
41. D O Scanlon, G W Watson, J Phys Chem Lett 1 3195 (2010)
42. J Robertson, Rep Prog Phys 69 327 (2006)
43. R Gillen, S J Clark, J Robertson, Phys Rev B 87 125116 (2013)
44. S J Clark, J Robertson, App Phys Lett 90 132903 (2008)
45. R Gillen, J Robertson, J Phys Conden Mat 25 165520 (2013)
46. W Monch, J App Phys 80 5076 (1996)
47. J Robertson, B Falabretti, J App Phys 100 014111 (2006)
48. P W Peacock, J Robertson, J App Phys 92 4712 (2002)
49. B Hoffling, A Schliefe, C Rodl, F Bechstedt, Phys Rev B, 85 035305 (2012)
50. A Schliefe, F Fuchs, C Rodl, J Furthmuller, F Bechstedt, App Phys Lett 94 012104 (2009)
51. M Cardona, N E Christensen, Phys Rev B 35 6182 (1987)
52. Y C Chang, Phys Rev B 25 605 (1982)
53. P H Dederichs, P Mavropoulos, O Wunnicke, N Papnikolaou, V Bellini, R Zeller, V Drchal, J Kudrnovsky, J Mag Mag Mater 240 108 (2002)
54. A A Demkov, L R C Fonseca, E Verret, J Tomfohr, O F Sankey, Phys Rev B 71 195306 (2005)
55. A W Cowley, S M Sze, J App Phys 36 3212 (1965)
56. E T Yu, J O McCaldin, T C McGill, Solid State Physics, 46 1 (Academic Press 1992),
57. A D Katnani, G Margaritondo, Phys Rev B 28 1944 (1983); G Margaritondo, Surf Sci 168 439 (1986)
58. W Chen, A Pasquarello, Phys Rev B 86 035134 (2012)
59. C Gong, H Zhang, W Wang, L Colombo, R M Wallace, K J Cho, App Phys Lett 103 053513 (2013)
60. J Kang, S Tongay, J Zhou, J Li, J Wu, App Phys Let 102 012111 (2013)
61. Y Guo, App Phys Lett 106 233104 (2016)
62. Y Guo, ACS Appl Mater Interfaces 7 25709 (2016)
63. H Li, J Robertson, J App Phys 115 203708 (2014)
64. C Kilic, A Zunger, App Phys Lett 81 73 (2002)
65. W Walukiewicz, Physica 302-303 123 (2001)
66. S B Zhang, S H Wei, A Zunger, 83 3192 (1998); A Zunger, App Phys Lett 83 57 (2003)